

Article

Impacts of Rainfall Variability, Land Use and Land Cover Change on Stream Flow of the Black Volta Basin, West Africa

Komlavi Akpoti ^{1,*}, Eric Ofofu Antwi ² and Amos T. Kabobah ²

¹ Faculty of Science and Techniques, Master Research Program of the West African Science Service Center on Climate Change and Adapted Land Use (WASCAL), Climate Change and Energy, University Abdou Moumouni of Niamey, P. O. Box 10662, Niamey, 8000, Niger

² Department of Energy and Environmental Engineering, University of Energy and Natural Resources, P. O. Box 214, Sunyani, Ghana; eric.antwi@uenr.edu.gh (E.O.A.); amos.kabobah@uenr.edu.gh (A.T.K.)

* Correspondence: akpotikomlavi@yahoo.fr; Tel.: +233-545-267-658

Academic Editor: Luca Brocca

Received: 4 May 2016; Accepted: 17 June 2016; Published: 4 July 2016

Abstract: Potential implications of rainfall variability along with Land Use and Land Cover Change (LULC) on stream flow have been assessed in the Black Volta basin using the SWAT model. The spatio-temporal variability of rainfall over the Black Volta was assessed using the Mann-Kendall monotonic trend test and the Sen's slope for the period 1976–2011. The statistics of the trend test showed that 61.4% of the rain gauges presented an increased precipitation trend whereas the rest of the stations showed a decreased trend. However, the test performed at the 95% confidence interval level showed that the detected trends in the rainfall data were not statistically significant. Land use trends between the year 2000 and 2013 show that within thirteen years, land use classes like bare land, urban areas, water bodies, agricultural lands, deciduous forests and evergreen forests have increased respectively by 67.06%, 33.22%, 7.62%, 29.66%, 60.18%, and 38.38%. Only grass land has decreased by 44.54% within this period. Changes in seasonal stream flow due to LULC were assessed by defining dry and wet seasons. The results showed that from year 2000 to year 2013, the dry season discharge has increased by 6% whereas the discharge of wet season has increased by 1%. The changes in stream flows components such as surface run-off (SURF_Q), lateral flow (LAT_Q) and ground water contribution to stream flow (GW_Q) and also on evapotranspiration (ET) changes due to LULC was evaluated. The results showed that between the year 2000 and 2013, SURF_Q and LAT_Q have respectively increased by 27% and 19% while GW_Q has decreased by 6% while ET has increased by 4.59%. The resultant effects are that the water yield to stream flow has increased by 4%.

Keywords: rainfall variability; Mann-Kendall test; Sen's slope; LULC; SWAT model; Black Volta; stream flow

1. Introduction

Assessing temporal trends and their spatial distribution pattern of precipitation remains a difficult task owing to their complex and non-linear nature in different regions. It is an important step for water resource projects in a basin. Rainfall distribution in Ghana, and West Africa in general, is influenced by the moist south-west monsoon and the dry north-east trade wind. Rainfall variability has a large influence on a water resource project. The eco-hydrological processes that influence the evolution of the surface ecosystem, depend on the spatio-temporal patterns of the precipitation and evapotranspiration (Oguntunde et al., 2006) [1]. Furthermore, land use and cover are changing fast in basin due to population growth and economical activities development in the basin.

Although the causes of rainfall variability may come from more global phenomena, it is important to know and understand their historical patterns or trends for better decision making. Changes precipitation may affect positively or negatively evaporation over the basin with the corresponding effect on stream flow. Rainfall changes may also affect directly river flow. (Conway et al., 2009) [2] studied rainfall and water resources variability in sub-Saharan Africa during the twentieth century. Their analysis of rainfall-runoff relationships reveals varying behavior including strong but non stationary relationships particularly in West Africa with rainfall accounting for around 60%–70% of river flow variability. (Mahe et al., 2001) [3] assessed the trends and discontinuities in regional rainfall of West and Central Africa from 1951–1988. Their results showed that the whole of West Africa, West of the Atakora Mountains experiences the more severe drought that has been observed in the majority of the stations. In Ghana for instance, their analysis revealed that there was a significant decreasing trend in standardized annual rainfall over the period 1951–1989. Using gridded monthly precipitation data available at 0.5 deg intervals over the period 1951–2000, (Owusu and Waylen, 2009) [4] showed that Africa has undergone a period of diminished rainfall with an apparent shift in the rainfall regime towards a longer dry season. (Logah et al., 2013) [5] analyzed rainfall pattern in Ghana showing high and low rainfall distribution in the country. Their results showed that between the period 1981–2010, there was a general decline in mean annual rainfall with high rainfalls shifting to the south-western corner of the country. Consequently, the agricultural production potential in the northern Ghana is diminished by high rainfall variability while the mean annual rainfall totals in all agro-ecological zones experienced a decline in precipitation [4]. The Mann-Kendal statistic was applied by (Oguntunde et al., 2006) [1] to assess trends and variability of hydro-climatology of the Volta basin in West Africa from 1901 to 2002. The results showed that a 10% relative decrease in precipitation resulted in a 16% decrease in runoff between 1936 and 1998. The Mann-Kendal test has also been used by (Lacombe et al., 2012) [6] when assessing drying climate in Ghana over the period 1960–2005. Their analysis showed no significant changes in the annual rainfall but reduction in the number of wet season days, a delay in the wet season onset at several locations throughout the country and lengthening of rainless periods during wet season. A water balance study of the Volta basin by (Andreini et al., 2000) [7] showed that runoff is extremely sensitive to rainfall therefore has significant impact on the hydropower generation.

The climate and Physical characteristics of the basin (such as topography, soil, vegetation and vegetation) as well as human activities are the main factors that influence the hydrological processes in basins. Among the foregoing models, physically based distributed models are well established models for analyzing the impact of land management practices on water, sediment, and agricultural chemical yields in large complex watersheds. Soil and Water Assessment Tool (SWAT) is a comprehensive, semi-distributed river basin model that requires a large number of input parameters, which complicates model parameterization and calibration [8]. As semi-distributed physically based simulation model, SWAT can predict the impacts of LULC and management practices on hydrological regimes in watersheds with varying soils, land use and management conditions over long periods and primarily as a strategic planning tool [9]. The SWAT model operates on a daily time step and is designed to predict the impact of land use and management on water, sediment, and agricultural chemical yields in ungauged watersheds [8]. The SWAT model application has gained reliability and consistency. It has been used worldwide because of its applicability in many aspects of water resource projects. Many models are being developed but physically based semi-distributed models such as SWAT are well established models for analyzing the impact of land management practices on water, sediment, agricultural chemical yields in large complex watershed [10]. For instance, in the case of watershed management program for conservation and development, runoff is one of the most important phenomena of hydrological cycle. The SWAT Model has been used for the estimation of surface runoff in India [11]. It has also been applied to model a hydrological water balance [12]. Sensitivity analysis has been performed by using the SWAT model for daily stream computation in Kentucky watershed [13].

The Volta Basin is one of the major river systems in Africa. Due to the importance of its contribution to the riparian countries economy, the use of hydrological model has become important in its water management. The SWAT model has been applied for some case studies within the basin. For instance, (Awotwi et al., 2015) [14] used the SWAT model to assess the impact of climate changes on water balance components of the White Volta. The results of this study suggested that change in rainfall leads to corresponding change in all the water balance components. The model was used to estimate groundwater recharge in the White Volta river basin [15]. The results of the study showed that the White Volta water balance indicates an important increase in the mean annual discharge, surface runoff and shallow groundwater recharge. According to the same results, the model shows that about 11% of the annual precipitation in the White Volta Basin becomes discharge, which consists of 4% surface runoff and 7% base flow. On a larger scale, the SWAT model was used to address calibration and uncertainties in West Africa including the basins of river Niger, Senegal and Volta [16]. The results showed that SWAT can be used for large-scale water investigations.

Although several studies have been conducted on rainfall variability impacts on water resources, only little research has been conducted on the spatial distribution of the trends in time series, especially at a basin scale. The objectives of this study over the Black Volta are to: (i) reveal the spatial pattern of the precipitation series using the aridity index (AI) profile of the basin, the standardized precipitation index (SPI), to explore the trends and its spatial distribution as well as its strength by the Mann-Kendall and Sen's slope estimator methods; (ii) assess land use and land cover change (LULC) in the basin over the last three decades; (iii) model river flow based on LULC and rainfall variability.

2. Materials and Methods

2.1. Study Area Presentation

The Black Volta basin lies between Latitude $7^{\circ}00'00''$ N and $14^{\circ}30'00''$ N and Longitude $5^{\circ}30'00''$ W and $1^{\circ}30'00''$ W, and covers an estimated area of about 130,400 km². The Black Volta river basin is a trans-boundary river system that stretches from Mali, Burkina Faso, Ghana and Cote d'Ivoire (Figure 1). In the year 2000, the Black Volta was home to about 4.5 million people and the population density in the basin ranges from 8 to 123 people/km² with Lawra district in Ghana having the highest density. This population is estimated to be about 8 million by the year 2025 [17].

According to [18], the population growth rate in the basin is about 3% a year. In the Black Volta, the major land use is agriculture. The major farming system in the sub-basin is bush fallow, which is extensive. In the north of the basin, particularly the Lawra district (Ghana section), lands are highly degraded both in terms of physical status and fertility levels and can therefore hardly support meaningful crop cultivation [19]. Previous study showed that most of the land in Ghana is under tree cover and crop land whereas artificial surface and associated areas are few. This gives an opportunity for development of agricultural activities in the Ghana section. In contrast, most of the land in Burkina Faso seems to be developed for food production with very little tree cover in the southern part. In fact, the vegetation zones are oriented from north to south, from the sparsely vegetated Sahel, to savannah regions, and the Guinea forest zone or rainforest in the extreme South. The dominant soils in the Black Volta basin according to the FAO soil classification are Luvisols and Gleysols with altitudes ranging between 60 m and 762 m above sea level [17]. In the Black Volta basin, the rainfall is highly variable in time and space. According to [20], it ranges respectively from 400 mm/year in the North to 1500 mm/year in the South. Over 70% of the annual total rainfall occurs in the months of July, August and September, with a little or no rainfall in the months of November to March in most parts of the basin. Mean monthly potential evapotranspiration exceeds mean monthly rainfall for most of the year for the entire basin.

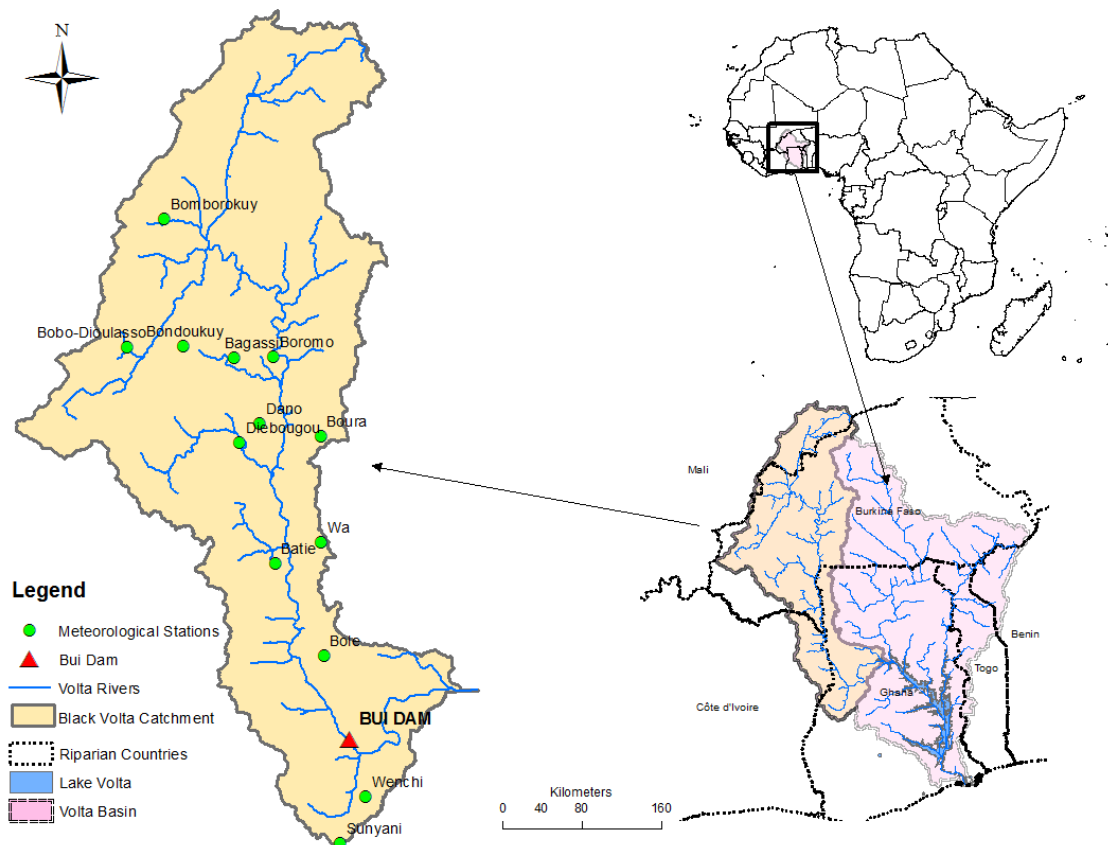


Figure 1. Study Area Presentation.

2.2. Rainfall Data Analysis

In order to reveal the trend of the annual total precipitation and its spatial distribution of the temporal trends in the Black Volta, three different approaches were applied as described in the following sections. Firstly, the aridity index profile of the basin was developed to describe the overall climatic zones of the basin. Secondly, the rainfall evolution of the basin was assessed by the standardized precipitation index. Finally, the spatial distribution of the trend and its statistical significance was analyzed by the Mann-Kendall and Sen's slope methods.

In climate data analysis, several methods have been developed for continuity and consistency checking [21,22]. For this study, the double mass curve method has been applied to the in situ rainfall data. The double mass curve is used to check the consistency of rainfall data by comparing data for a single station with that of a pattern composed of several other stations in the study area [23]. The point plotted in the double mass curve were fitted closely in a straight line showing that there was no or was minimum error in data processing, and there was no change in data collection method. The rainfall data for thirteen stations was collected from the Ghana Meteorological Agency (GMA), the Direction General de la Meteorologie du Burkina Faso and Global Climate Data. Table 1 shows the general characteristics of the study stations and their country locations in the trans-boundary Black Volta basin.

2.2.1. Aridity Index

The Aridity Index (AI) map was developed using the Global Aridity Index dataset collected from Global Aridity and Potential Evapotranspiration (PET). (See Appendix A for more details).

2.2.2. Standardized Precipitation Index

The standardized precipitation index SPI_{sy} is a normalized index representing the probability of occurrence of an observed rainfall amount when compared with the rainfall climatology of a given station (see Appendix A for more information).

Table 1. General characteristics of the study stations and their country locations.

Country	Gauging Station	Lat (°N)	Lon (°W)	Elevation (m)
Ghana	Sunyani	7.3328	−2.3281	296
Ghana	Wenchi	7.75	−2.1	322
Ghana	Bui	8.2361	−2.2772	176
Ghana	Bole	9.0319	−2.4762	295
Ghana	Wa	10.0667	−2.5	262
Burkina Faso	Batie	9.8739	−2.9213	298
Burkina Faso	Diebougou	10.9667	−3.25	298
Burkina Faso	Boura	11.0333	−2.5	306
Burkina Faso	Dano	11.1490	−3.2931	304
Burkina Faso	Boromo	11.75	−2.9333	260
Burkina Faso	Bondoukuy	11.8450	−3.7639	326
Burkina Faso	Bobo-Dioulasso	11.1605	−4.3298	374
Burkina Faso	Bomborokuy	12.9972	−3.9496	344

2.2.3. Mann-Kendall Trend Test

In hydrology and climatology, the tests for trend detection in time series data can be considered as parametric test and non-parametric test. The parametric test requires the data to be normally distributed and independent while the data is required to be only independent for non-parametric test. In the present paper, two ranked non-parametric tests have been used for detecting monotonic trends in the rainfall time series data. They are namely Mann-Kendall trend test and Sens slope estimator. The Mann-Kendall test has been widely used in hydrology and climatology for trend detection [24–28]. There are some advantages using this test. It is not required data to be normally distributed. The results of the test are not affected by the existence of outliers in the data [29] or inhomogeneous time series. The test statistic distribution was derived by (Kendall, 1962) [30]. In the trend, the null hypothesis H_0 assumes that there is no trend in the rainfall time series data over a given period and it is tested against the alternative hypothesis H_1 which considers that there is increasing or decreasing trend [31]. The theoretical calculation of the Mann-Kendall statistic can be seen in Appendix A.

2.2.4. Sen's Slope Estimator

The Sen's slope estimator has been widely used in hydro-climatology to estimate the true slope in time series data wherever it exists [32–34]. The true slope, which is the change per unit time can be computed based on the non-parametric method developed by [35]. (refers to Appendix A for theoretical background).

2.3. Land Use and Land Cover Change Maps Development

In order to assess land use and land cover change (LULC) in the Black Volta catchment, three land cover maps were developed based on satellite image bands combination. The years 1987, 2000 and 2013 Landsat images were collected corresponding to 28 years' period. The Landsat 5 thematic mapper (TM) sensor data was processed for the year 1987, the Landsat 7 SLC-on was processed for the year 2000 while the year 2013 data was collected from the Landsat 8 Operation Land Image (OLI). In order to minimize classification error and differences in the vegetation growth throughout the year, all the data were collected for the month of January and the cloud cover is set to zero. All Landsat data were at 30 m resolution. These satellite data are produced by the United States Geological Survey

(USGS) and freely available from the USGS Global Visualization Viewer (USGS GLOVIS) platform (<http://glovis.usgs.gov/>). For the Black Volta, 14 scenes were necessary to cover the entire basin which correspond to the following Path/Row: 194/54, 195/55, 195/54, 195/53, 195/52, 195/51, 196/54, 196/53, 196/52, 196/51, 196/0, 197/53, 197/52, 197/51.

The supervised maximum likelihood classification method was used to develop the land use classes. The method is time consuming due to the training sample selections and the possibility to confuse some classes. The images were processed in ArcGIS software. The color balancing is also identified as main challenge, is the mosaic of all combined bands. The classification was performed in comparison to previous land use classes identified in the basin [17]. The classification was also validated using Google Earth since it can give better visualization of the land cover types on the ground. Seven classes of land use and land cover classes were selected or identified: Water bodies, bare land, Urban areas, forest evergreen, forest deciduous, agricultural land and grass land.

The thematic map is an efficient approach to derive information from an image. However, it is also subjected to error, which can be geometric errors, incorrectly training sample labeling before supervised classification, unidentified classes, etc. A statistical approach to quantify these errors is the random selection of pixels from the classification map and comparing them to the reference map, which produces a confusion matrix. A confusion matrix has been widely used for accuracy assessment of the land use land cover maps [36–39]. The main statistical information derived from the confusion matrix are overall accuracy, commission error, omission error, the producer's accuracy, the user's accuracy and Kappa Coefficient K. The overall accuracy is the total accuracy of the classification. The Kappa coefficient is a discrete multivariate technique of use in accuracy assessment. $K > 0.8$ usually considered as strong agreement and good accuracy [40].

2.4. Brief Description of the SWAT Model

The Soil and Water Assessment Tool (SWAT) is a semi-distributed physical based model. It was developed by the United States Department of Agriculture (USDA) Agricultural research Service (ARS) to predict the impact of land use practices on water, sediment and agricultural chemical yields in large and complex watersheds with varying soils, land use and management conditions over long period [41]. SWAT is a continuous time or long term yields model where the model is not designed to simulate detailed, single-event flood routing. The model simulation is daily time step based. The spatial complexity of the watershed is taken into account in the model by combining the information from Digital Elevation Model (DEM), soil and land use. The SWAT model divides the watershed into sub-basins. The sub-basins are further subdivided into hydrological response units based on the land used and soil distribution. The model is divided into eight major components including hydrology, weather, sedimentation, soil, temperature, crop growth, nutrients, pesticides and agricultural managements. Water balance is the driving force behind everything that happens in the watershed. According to [41], the hydrology of the watershed can be separated into two major divisions: the first division is the land phase of the hydrologic cycle and the second division is the water or routing of the hydrologic cycle. The land phase of the hydrologic controls the amount of water, sediments, nutrients and pesticides loading to the main channel in each sub-basin. The movement of water, sediments, nutrients and pesticides through the channel network to the watershed outlet is considered as the routing phase. The SWAT's simulation of the hydrologic cycle is based the following water balance equation [41]:

$$SW_t = SW_o + \sum_{i=1}^t (R_{day} - Q_{surf} - E_a - W_{seep} - Q_{wg}) \quad (1)$$

where: SW_t is the final soil water content (mm H₂O), SW_o is the initial water content on day i (mm H₂O), t is the time (days), R_{day} is the amount of precipitation on day i (mm H₂O), Q_{surf} is the amount of surface runoff on day i (mm H₂O), E_a is the amount of evaporation on day i (mm H₂O),

W_{seep} is the amount of water entering in the vadose zone from the soil profile on day i (mm H₂O), Q_{gw} is the amount of return flow on day i (mm H₂O).

2.4.1. Surface Runoff

Overland flow or surface runoff consists of flow along a sloping surface. SWAT provides two methods for modeling surface runoff: The Soil Conservation Service (SCS) curve number method [42] and the Green and Ampt infiltration method [43]. SWAT simulates surface runoff volume and peak rates for each HRU based on these two methods. The curve number method is daily based time step when used for computing surface runoff in the SWAT and it is unable to compute directly infiltration. Rather, the amount of water entering the soil is computed as the difference between the amount of rainfall and the amount of surface runoff. On the other hand, the Green and Ampt infiltration method compute directly the infiltration in the model but requires data in sub-daily increments [41]. The method used for this work is the curve number method due to the daily based data that we have for the project. The curve number equation is given by (SCS, 1972) [42] as:

$$Q_{\text{surf}} = \frac{(R_{\text{day}} - I_a)^2}{(R_{\text{day}} - I_a + S)} \quad (2)$$

where: Q_{surf} is the accumulated runoff (rainfall excess) in (mm H₂O), R_{day} is the rainfall depth for the day (mm H₂O), I_a is the initial abstraction which includes surface store, interception and infiltration prior to runoff (mm H₂O), S is the retention parameter (mm H₂O) and it is defined as:

$$S = 25.4 \left(\frac{1000}{\text{CN}} - 10 \right) \quad (3)$$

where CN is the curve number for the day. I_a is commonly given as $0.2 S$. Hence Equation (2) becomes:

$$Q_{\text{surf}} = \frac{(R_{\text{day}} - 0.2S)^2}{(R_{\text{day}} + 0.8S)} \quad (4)$$

Runoff is generated only when $R_{\text{day}} > I_a$. Typical curve number for moisture conditions are classified into four hydrological groups such as: A for high infiltration, B for moderate infiltration, C for slow infiltration and D very slow infiltration. According to the U.S. National Resource Conservation Service (NRSC) Soil Survey Staff, a hydrologic group is defined as a group of soil having similar runoff potential under the similar storm and cover conditions [44]. The full description of the other components of the SWAT model can be find in the theoretical documentation of the SWAT model [41].

2.4.2. Model Input

Digital Elevation Model

The DEM data for this study was 90 m resolution from the Shuttle Radar Topographical Mission (STRM). The DEM was used for watershed delineation including stream definition, outlets and inlets definitions as well as calculation of the sub-basins parameters. The slopes definition in the basin was also based on the DEM. The DEM map of the study area can be seen in the Figure 2a.

Soil Data

The soil data was collected from the FAO soil database. The importance of the soil data in the model is due to the fact that it allows the determination of the soil texture, available water content, hydraulic conductivity, bulk density and organic carbon content for different layer according to each soil type. For the Black Volta, the dominant soil types are illustrated in Figure 2b according to the SWAT database code and the FAO soil unit classification.

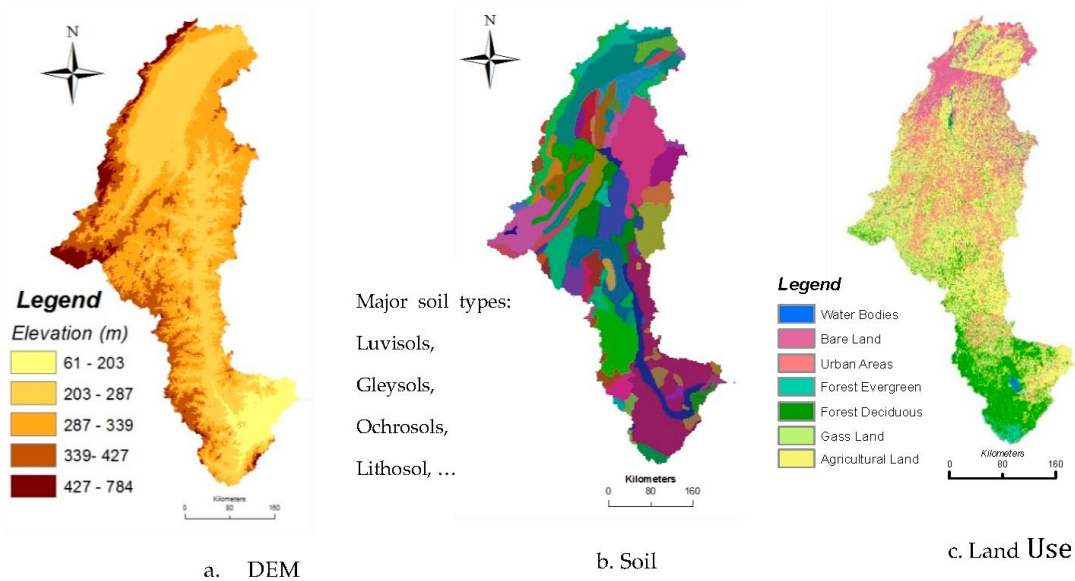


Figure 2. Geographical Information System (GIS) and Satellite Input Data.

River Discharge

The stream flow data used in this work corresponds to a monthly stream flow data of the Black Volta measured at Bui from 1954 to 2010. The data was collected from the Bui Power Authority (BPA). The maximum flows are observed in the months of August, September and November. The annual average, maximum, minimum and coefficient of variation of flow for all the months of the period 1954–2010 are respectively $227.6 \text{ m}^3/\text{s}$, $612.2 \text{ m}^3/\text{s}$, $70.7 \text{ m}^3/\text{s}$ and 40%.

2.4.3. Black Volta Basin Model Set Up

As a hydrological model, the starting point of the SWAT database creation is the watershed definition. The slopes and elevations were also generated as a topographical parameter of the watershed using the DEM as an important factor for the basin. The slopes in combination with soil and land use control the surface runoff. In this work, five slopes classes were defined as follow: 0%–2%, 2%–4%, 4%–10%, 10%–15% and greater than 15%. The highest elevation of the basin is 784 and the smallest is 79 m above mean sea level. Each sub-basin in the watershed is divided into units called hydrological response units (HRUs) [41]. For the Black Volta, 382 HRUs were created for the 17 sub-basins. In the SWAT model, there are three types of HRU definition options including dominant land use, soils, slope, dominant HRU and multiple HRU option. In this work, multiple HRUs option was chosen. Land use class percentage over sub-basin areas was set to 15%, soil class percentage over land use area was 5% and slope class percentage over soil area was 15%.

Soil and Water Assessment Tool-Calibration and Uncertainty Programs (SWAT-CUP) is an automated calibration model which provides link between the input/output of a calibration program and the model. The sensitivity analysis was performed in two ways: first by varying one parameter at a time while keeping the others constant, second by varying all the parameters simultaneously. The flow chart of the SWAT modeling is depicted in Figure 3.

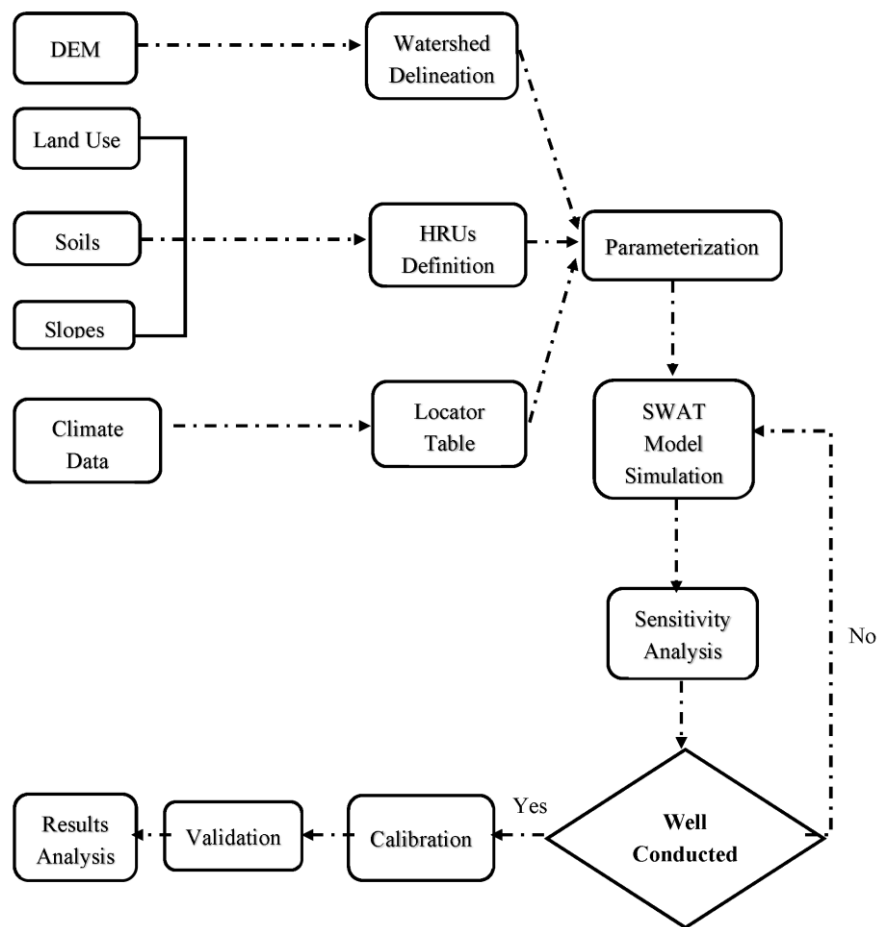


Figure 3. Flow Chart of the Steps in the SWAT Model Application in the Black Volta Basin.

The type of change to be applied to the parameter in the model is defined by the code $r_{_}$, $v_{_}$, and $a_{_}$. According to (Abbaspour et al., 2007) [45], $r_{_}$ means the existing parameter value is multiplied by $(1 + \text{a given value})$, $v_{_}$ means the default parameter value is replaced by a given value, $a_{_}$ means a given quantity is added to the default value. The Sequential Uncertainty Fitting (SUFI-2) model by (Abbaspour et al., 2004) [46] for optimization and uncertainties analysis was used in the SWAT-CUP for calibration and validation. The Nash-Sutcliffe (SN) coefficient [47] was assigned as the objective function. In SUFI-2, a parameter uncertainty is propagated (as uniform distribution) through a Latin Hypercube (statistical method for generating a sample of plausible collections of parameter values from a multidimensional distribution) sampling [16]. It is referred to as the 95% depicting prediction uncertainty or 95PPU (known as P-factor) calculated at 2.5% and 97.5% levels for each parameter. The 95PPU is the degree to which all uncertainties are accounted for [48]. The average thickness of the 95PPU band divided by the standard deviation of the measured data quantify the strength of the calibration and uncertainty analysis is known as R-factor. The perfect situation would be 100% of the observed data bracketed in the 95PPU while at the same time R-factor is close to zero [48]. SUFI-2 account for all uncertainties including uncertainties in the driving variable, like rainfall, conceptual model, parameters and measured data. Two sets of calibration and validation were performed based on the land use of the year 2000 and 2013. The first calibration covered the period 2000–2005 and the validation for the period 2006–2010 using the 2013 land use data. The 2013 Landsat 8 data was used assuming that within 3 years, there were not significant changes in the basin. The second calibration was performed for the period 1990–1995 and the validation for the period 1996–2000 using the land use data of the year 2000.

For the model evaluation, two most widely statistical test in hydrology are considered:

- i Goodness of fit or coefficient of determination (R^2) between the observation and the final best simulation:

$$R^2 = \frac{\sum_{i=1}^n (Q_{\text{obs},i} - \bar{Q}_{\text{obs}})(Q_{\text{sim},i} - \bar{Q}_{\text{sim}})}{\left[\sum_{i=1}^n (Q_{\text{obs},i} - \bar{Q}_{\text{obs}})^2 \right]^{0.5} \left[\sum_{i=1}^n (Q_{\text{sim},i} - \bar{Q}_{\text{sim}})^2 \right]^{0.5}} \quad (5)$$

- ii And the Nash-Sutcliffe (NS) coefficient (Nash et al., 1970) [47]:

$$NS = 1 - \frac{\sum_{i=1}^n (Q_{\text{sim},i} - Q_{\text{obs},i})^2}{\sum_{i=1}^n (Q_{\text{obs},i} - \bar{Q}_{\text{obs}})^2} \quad (6)$$

where: $Q_{\text{obs},i}$ is the observed flow at time i (m^3/s), \bar{Q}_{obs} is the mean of observed flow (m^3/s), $Q_{\text{sim},i}$ is the simulated flow at time i (m^3/s), \bar{Q}_{sim} the mean of simulated flow (m^3/s). The Nash-Sutcliffe coefficient rating on monthly time step is given by (Moriassi et al., 2007) [49]. (Awotwi et al., 2015) [14] stated that for model the calibration to be accepted, R^2 should be greater than 0.6 and the NS greater than 0.5.

For the model evaluation, two most widely statistical tests in hydrology are considered: Goodness of fit or coefficient of determination (R^2) between the observation and the final best simulation and the Nash-Sutcliffe (NS) coefficient [47]. The Nash-Sutcliffe coefficient rating on monthly time step is given by (Moriassi et al., 2007) [47]. (Awotwi et al., 2015) [14] stated that for model the calibration to be accepted, R^2 should be greater than 0.6 and the NS greater than 0.5.

3. Results and Discussions

3.1. Aridity Index Profile of the Black Volta and the Standardized Precipitation Index

The aridity index (AI) map of the Black Volta (Figure 4) shows that the basin has three climatic conditions: semi-arid, dry sub-humid and humid zone. The AI of the semi-arid zone varies from 0.2 to 0.46 and it is located in the northern part of the catchment (Burkina and Mali). For the dry sub-humid zone, the AI varies from 0.46 to 0.58 and it is located in the middle of the basin (Burkina Faso and Ghana). The humid zone that is the southern of the basin (Ghana and Ivory Coast) has AI between 0.58 and 0.84. More than the half of the basin is dry showing that atmospheric water demand cannot be met by precipitation. Similar results have been found in the case of the Volta Basin by [1]. The standardized precipitation index (SPI) was computed as an average of set of rainfall stations available in each climatic zone according to AI (Figure 4) with the same rainfall trends (see Table 2). Figure 5a presents the SPI of stations Bondoukuy, Bobo-Dioulasso and Boromo in the semi-arid zone. The results show that there was an apparent succession of dry periods, normal periods and wet periods. However, a close look at the graph revealed between 1976 and 1990, there was more drought years than wet years while from 1991 to 1999, the semi-arid zone experienced more wet condition showing an abrupt discontinuity of time series records. Finally, from the year 2000 to 2011, there were more severe drought conditions with only three years showing wet conditions. Figure 5b is an average of SPI from the stations Wa, Boura Diebouyou and Dano that represent the dry sub-humid zone (see Figure 4). The SPI showed a wet/normal condition from 1976 to 1980, a continuous drought condition from 1981 to 2005 and exclusively wet years from 2006 to 2011. One can say that the severity of drought has decrease from the year 1986 showing a recovery from drought to wet condition. The SPI of the humid zone from the stations Sunyani, Wenchi and Bole showed an alternation of wet and dry periods with more wet conditions from the year 2002. Although the SPI of each climatic zone differ from one another, there are some common characteristics: the year 1983 showed a singular very dry condition for all the three

climatic zones, there is a kind of recover from drought condition since the year 2000. This tendency is confirmed by Figure 5d, which is a regionalized SPI (the average of the SPI from the three climatic zones). Similar results were found in the previous research in the case of west Africa and Sahel [3,50].

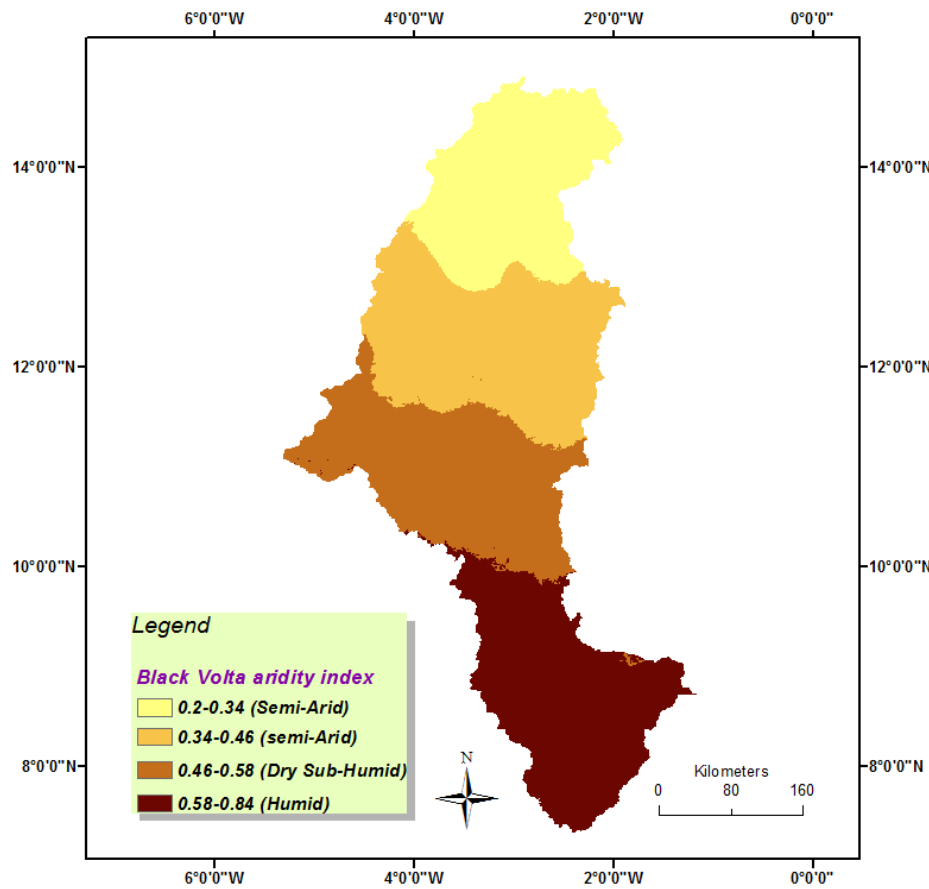


Figure 4. Aridity Index profile of the Black Volta Basin.

Table 2. Mann-Kendall Statistics and the Sen’s Slope Estimator.

Gauging Station	Tau	p-Value	Zs	Qs med or Sen’s Slope Estimator	Constant B
Sunyani	0.156	0.1864	1.321	0.3437	93.12
Wenchi	0.073	0.5399	0.6129	0.1197	101.68
Bui	−0.0724	0.4535	−0.7497	−0.1283	94.11
Bole	0.18	0.1271	1.55	0.3961	82.17
Wa	0.127	0.2819	1.076	0.1749	83.29
Batie	−0.0635	0.5953	−0.531	−0.1559	88.69
Diebougou	0.106	0.3686	0.899	0.1178	83.47
Boura	0.279	0.0171	2.38	0.3218	70.02
Dano	0.143	0.2254	1.21	0.222	72.03
Boromo	0.113	0.3403	0.954	0.1754	68.17
Bondoukuy	−0.132	0.6728	−0.422	−0.0936	71.85
Bobo-Dioulasso	−0.0635	0.5952	−0.5312	−0.1683	84.75
Bomborokuy	−0.126	0.2584	−1.13	−0.2106	62.73

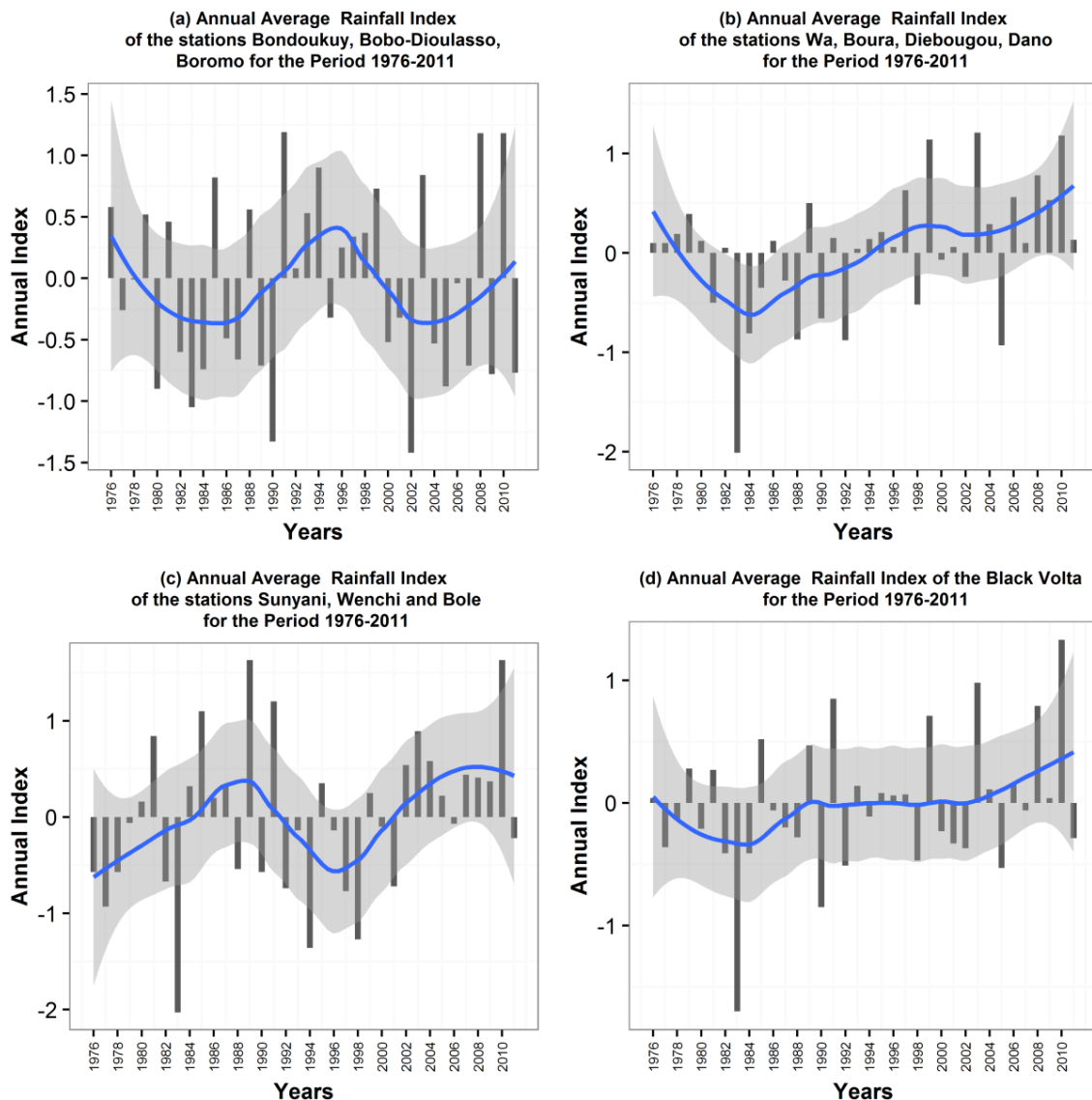


Figure 5. Annual Precipitation Index. The blue line or regression line represents a smoother (mean of Precipitation index at each year). The grey band is the display of confidence interval (95% confidence interval) around the smoother. This helps to see the overall trend in the precipitation index.

3.2. Rainfall Trend Analysis

In order to understand the rainfall variability for possible climate change detection in the basin, the Mann-Kendall trend test and the Sens estimator were applied to thirteen rainfall stations throughout the entire basin. The statistical indicators from the trend test are the Kendall tau, the standardized statistic Z_s , the p -value, and the Sens slope. The Kendall tau is a measure of correlation; therefore, measures the strength of the relationship between the two variables (time and rainfall) based on the rank of the data. The statistic Z_s and the p -value measures the significance of the trend while the Sens slope estimates the magnitude of the trend (similar to the tau value). The test was performed based on the annual average for the periods 1976–2011 that correspond to reliable data availability. The results are summarized in Table 2. The results showed that about 62% of the stations in the basin (that is eight out of thirteen) presented an increased trend in precipitation while 38% presented a decrease in precipitation (five stations out of thirteen). However very few of these trends are statically significant. In the humid zone of the Black Volta (that is Ghana and Ivory Coast), all the stations presented an increase in rainfall except for Bui. The analysis for Bui corresponded to the period

1954–2005. According to the Mann Kendall trend test, the tau value is -0.0724 while the Sens slope is -0.1283 suggesting a decrease in rainfall since 1954.

The p -value that is 0.4535 (greater than 0.05) suggested that although there is a decrease in rainfall, the trend is not statistically significant. This was confirmed by the statistic Z_s equals -0.7497 (weak compared to 1.96). Let's recall that as discussed in the theoretical background of the Mann-Kendall statistics, for the trend to be statistically significant, Z_s should be greater than 1.96.

3.3. Land Use and Land Cover Change Analysis

According to (Anderson et al., 1976) [51], the minimum level of interpretation accuracy in the identification of LULC categories from remote sensing data should be at least 85% while (Carletta, 1996) [40] states that the Kappa coefficient should be greater than 80%. Based on the results in Table 3, the classification used in this study fulfills the minimum acceptability level as defined above. The results in Table 3 showed that the Landsat images have been improved since 1987 (recent Landsat gives better results). In fact, the overall accuracy of LULC 1987 (Landsat 5 TM) is 90.2%, 93.06% for LULC 2000 (the Landsat 7 SLC-on) and 99.18% for LULC 2013 (Landsat 8 OLI). Similar results were found for the Kappa coefficient, which varies from 88.57% (1987) to 99.05% (2013). During the images classification, it was difficult some to distinguish between bare land in the extreme north of the catchment with semi-arid climatic condition from the urban areas in the catchment or agricultural land from grass land. In general, we can say that the land use maps are acceptable enough and can be used for land use changes analyses and projections in the basin.

Table 3. Overall Accuracy and Kappa Coefficient of the LULC Maps.

Year	Overall Accuracy	Kappa Coefficient
1987	90.20	88.57
2000	93.06	91.90
2013	99.18	99.05

Figure 6 shows LULC maps developed for the years 1987, 2000 and 2013 for the Black Volta in this project. The land use classes considered in this work are water bodies, bare land, urban areas, forest evergreen, forest deciduous, grass land and agricultural land. In general, agricultural and bare lands are dominantly in the Burkina Faso and Mali section of the basin while forest evergreen and deciduous are dominantly in the Ghana and Ivory Coast sections of the catchment. This agreed with previous work [17] in the basin. Table 4 summarizes the characteristics of each land use type according to the year.

The dominant land use types in the Black Volta catchment in the year 1987 (Figure 6a) were grass land (76,253.9 K. km²) and agricultural land (36,125.7 km²) representing respectively 47% and 22% (Table 4) of the total area of the basin. Forest evergreen and forest deciduous represent respectively 9% and 8%. Urban areas in 1987 occupied 6% of the Black Volta. Water bodies represent the smallest portion of the basin with an area of (101.7 km²) representing only 0.1% of the basin. In the year 2000, the Black Volta had grass land as dominant land cover type with 74,198.48 km²) representing 48% of the catchment followed by agricultural land (24%). Between 1987 and the year 2000, forest evergreen has decreased by 1% while water bodies has increased from 0.1% in 1987 to 0.6% in year 2000. Urban areas also have increased significantly. The year 2013 was characterized by the dominance of the agricultural land with an area of 47,710.41 km² representing 31% of the catchment area while grass land has decreased up to 41,151.37 km² (26%). We also notice a significant increase in urban areas (14%) and forest deciduous (15%). Table 4 summarizes the land use changes and rate of change from 1987 to 2013. Between 1987 and 2000, forest evergreen has decreased about 83.05% (5.93%/year).

If we consider the period 2000–2013, agricultural land has increased by 29.66% (2.12%/year) while urban areas have increased by 33.22% corresponding to +2.37% each year. If we consider the evolution of the land use classes conserved in this study from 1987 to 2013, the results showed that grass land

and deep forest proportions have decreased at a rate of 1.70% and 2.84% each years. This makes sense when we observed for the same period (1987–2013), an increase of urban areas (4.78%/year) and agricultural land (1.19%/year). We also have noticed an important evolution in water bodies (30.5%/year). This important increased trend might be due to the Bui dam construction. Note that this important development of water bodies represents only 0.61% of the total basin area in the year 2013. We can say that urbanization and deforestation are taking place very fast in the Black Volta catchment with possible implications for hydrology the basin.

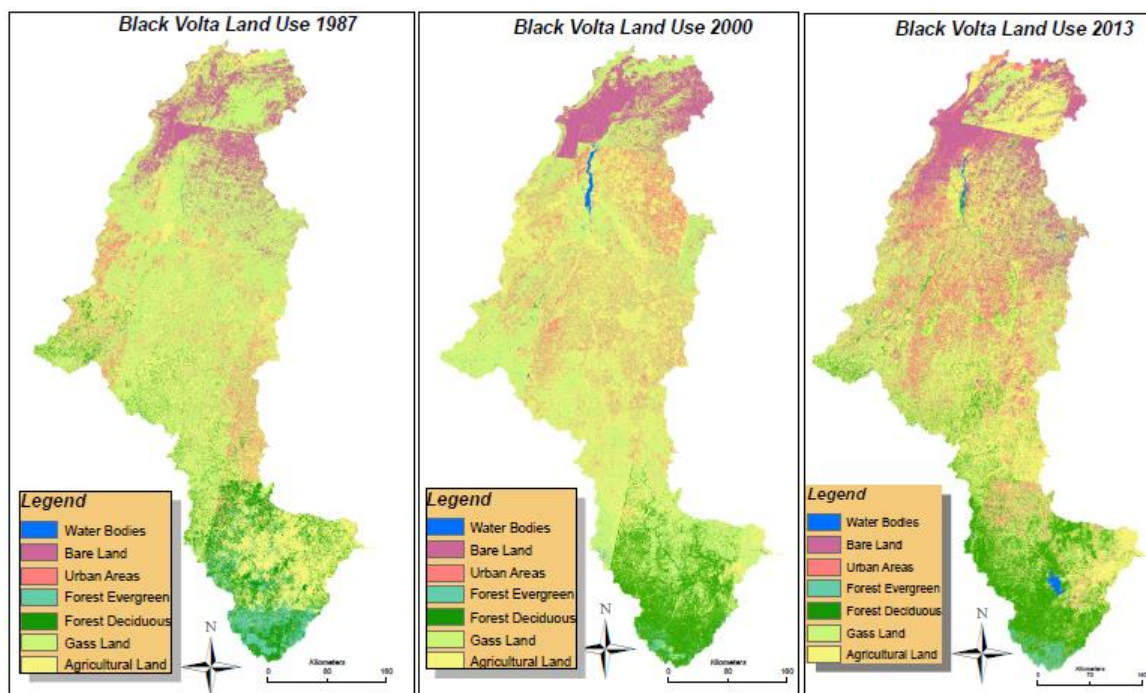


Figure 6. LULC maps of the Black Volta. (a) LULC 1987; (b) LLULC 2000; (c) LULC 2013.

3.4. SWAT Modeling Results

3.4.1. Sensitivity Analysis

The definition and the significance of each SWAT parameters were presented in the Table 5. Although several parameters were tested during the modeling of the Black Volta catchment, twelve were finally found to be the most sensitive. The summary of the most sensitive parameters is presented in Table 5 as well as their final range from the last iteration in SUFI-2, the fitted values and the sensitivity rank. Sensitivity of parameters is calculated by a multiple regressive system using the Latin hypercube generated parameters against the objective function [48]. The objective function in this study was the Nash-Sutcliffe coefficient. Parameter ranking is based on the t-test and the p -value in the SUFI-2 program. T-test gives a measure of the sensitivity meaning the larger the t-test in absolute value, the more sensitive the parameter is while the p -value determined the significance of the sensitivity [48]. P -value closed to zero are more sensitive. Among the twelve final parameters, the six most sensitive including saturated hydraulic conductivity (SOLK), time constant for low flow (MSKCO2), time constant for normal flow (MSKCO1), Surface runoff lag time (SURLAG), Available water capacity of the soil layer (AWC), and the curve number (CN2). Most of these parameters are soil and land use land cover related, hence it calls for paying particular attention to soil and land use management practices in the basin.

Table 4. LULC trends.

Land Cover Type	Area Coverage (km ²)			Area Coverage (%)			1987–2000		2000–2013		1987–2013	
	1987	2000	2013	1987	2000	2013	Change (%)	Change Rate (%/year)	Change (%)	Change Rate (%/year)	Change (%)	Change Rate (%/year)
Bare Land	13231.9	11279.37	18842.86	8.5	7.3	12.15	−14.76	−1.05	67.06	4.79	42.4	1.57
Urban Areas	9619.8	16537.32	22030.4	6.2	10.7	14.21	71.91	5.14	33.22	2.37	129.01	4.78
Water Bodies	101.7	872.6904	939.15	0.1	0.6	0.61	758.1	54.15	7.62	0.54	823.45	30.5
Agricultural Land	36125.7	36796.48	47710.4	23.3	23.7	30.77	1.86	0.13	29.66	2.12	32.07	1.19
Grass Land	76253.9	74198.44	41151.4	49.2	47.9	26.54	−2.7	−0.19	−44.54	−3.18	−46.03	−1.7
Forest Deciduous	14034.6	14398.31	23063.6	9.1	9.3	14.87	2.57	0.19	60.18	4.3	64.33	2.38
Forest Evergreen	5708.9	967.4019	1338.64	3.7	0.6	0.86	−83.05	−5.93	38.38	2.74	−76.55	−2.84

Table 5. Most Sensitive Parameters.

Parameter Name	Definition	Absolute SWAT Values	Fitted Value	Minimum Value	Maximum Value	Sensitivity Rank
R_SOL_K	Saturated hydraulic conductivity	0–2000	−0.999737	−1.009404	−0.966056	1
V_MSK_CO2	Calibration coefficient used to control impact of the storage time constant for low flow	0–10	3.117479	2.870465	5.470611	2
V_SURLAG	Surface runoff lag time	0.05–24	22.728235	22.493849	22.75284	3
V_MSK_CO1	Calibration coefficient used to control impact of the storage time constant for normal flow	0–10	10.726233	9.479877	14.147874	4
R_SOL_AWC	Available water capacity of the soil layer	0–1	0.201121	0.145896	0.2093	5
R_CN2	SCS runoff curve number f	−0.2–0.2	−0.537993	−0.552411	−0.505139	6
A_GWQMN	Threshold depth of water in the shallow aquifer required for return flow to occur (mm)	0–5000	73.4655	73.35611	74.378479	7
V_ALPHA_BF	Base flow alpha factor (days)	0–1	−0.155831	−0.160484	−0.153358	8
V_GW_DELAY	Groundwater delay (days)	0–500	1.087874	0.994085	1.122037	9
V_RCHRG_DP	Deep aquifer percolation fraction	0–1	0.159342	0.148055	0.176487	10
V_ESCO	Soil evaporation compensation factor	0–1	0.599675	0.595305	0.646715	11
V_CH_N2	Manning's "n" value for the main channel	−0.01–0.3	0.267461	0.242134	0.271966	12

3.4.2. Calibration and Validation

Although the SWAT model was set up based on daily data, the calibration and validation at Bui were based on average monthly data (only monthly data was available). Two sets of calibration and validation were performed (the period covering the Bui dam construction and before the dam construction). The final parameters and their fitted values are summarized in Table 5. Although the minimum and the maximum values of these parameters as are closed, these parameters agreed in general with previous SWAT modeling in the Black Volta basin and in West Africa [14,16,52]. The first calibration was performed for the period 2000–2005 and the first validation for the period 2006–2010 (Figure 7a). The performance of the model for this first calibration and validation is summarized in Table 6. The model performance during calibration and validation can be qualified as very good based on the general performance ratings for recommended statistics for a monthly time step given by (Moriassi et al., 2007) [49]. The calibration showed that, the objective function which is the Sutcliffe coefficient (NS) is 0.90 while the goodness of fit between the measured and the simulated R^2 is also 0.91. The strong correlation between the measured flow and the simulated (Figure 8a) showed that the physical processes implicated in the generation of stream flow in the Black Volta catchment are well captured by the model during calibration. However, the model overestimated the simulated average monthly flow ($252.70 \text{ m}^3/\text{s}$) compared to the measured ($223.16 \text{ m}^3/\text{s}$) during calibration while it is underestimated simulated standard deviation ($274.3 \text{ m}^3/\text{s}$) compared to the measured standard deviation ($306.38 \text{ m}^3/\text{s}$). Model performance during validation (Figure 7b) can be qualified as good. The NS was 0.70 while R^2 was 0.80 (Figure 8b).

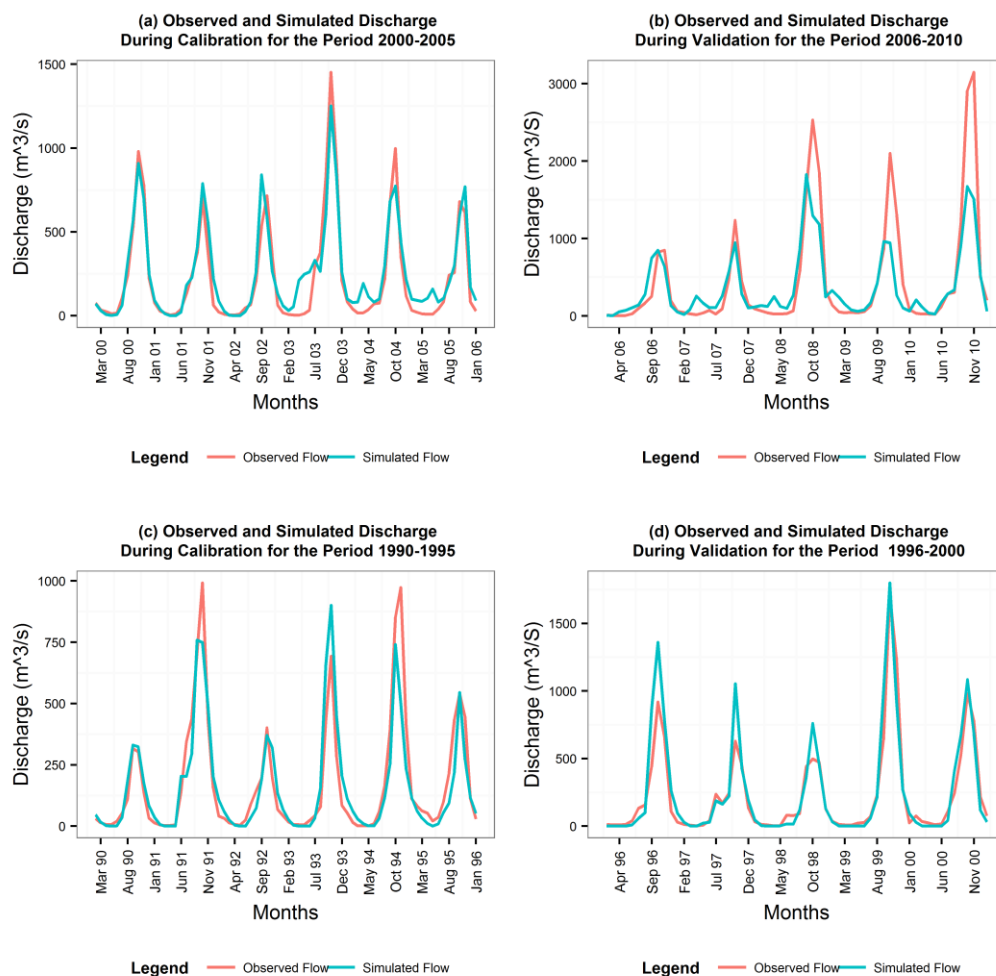


Figure 7. Discharge during Calibration and Validation.

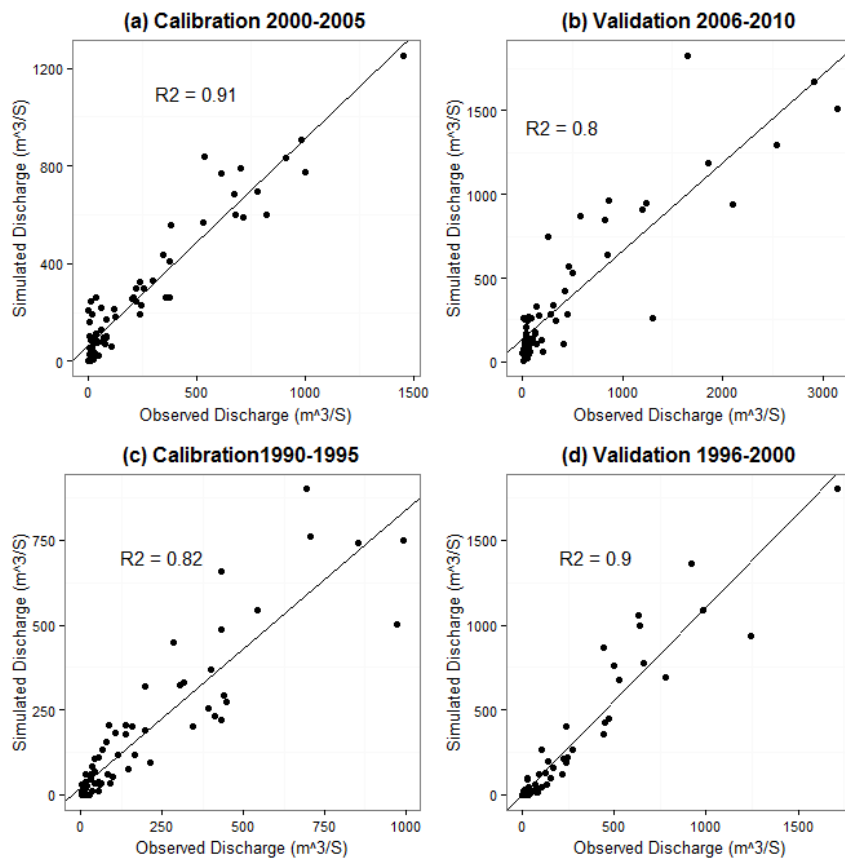


Figure 8. Simulated Discharge vs. Observed Discharge.

Table 6. Model performance During the Period 2000–2010.

Period	Average Monthly Flow (m ³ /s)		Standard Deviation (m ³ /s)		Model Performance			
	Measured	Simulated	Measured	Simulated	P-Factor	R-Factor	R ²	NS
Calibration (2000–2005)	223.16	252.70	306.38	274.3	0.64	0.66	0.91	0.9
Validation (2006–2010)	447.99	371.23	730.94	433.84	0.2	0.33	0.80	0.7

Similar results are observed for standard deviations. The simulated standard deviation (433.84 m³/s) was underestimated compared to the observed one (730.94 m³/s). A close look at the Figure 7a revealed that the peak flows during calibration were correctly modeled while Figure 7b during validation showed a delay in peak flows from August 2008. The simulated peak flows are much lower than the observed peaks. One of the major reasons behind this result is the assumption that the construction of the Bui Dam disturbed the dynamism of the flows. According to the Bui Power Authority (BPA), the diversion of the Black Volta River was completed in December 2008 and the construction of the main dam began in December 2009. Similar effects have been reported by (Schuol and Abbaspour, 2006) [16] on the Niger River where construction of a reservoir is said to delay the river flows. To confirm this hypothesis in our case, a second set of calibrations and validations have been performed prior to the Bui dam construction.

The second calibration and validation (Figure 7c, d) were performed respectively for the period 1990–1995 and 1996–2000 with the same number of years as it was for the first calibration and validation (five years for calibration and four years for validation). The results are summarized in Table 7. The performance of the model during calibration can be qualified as very good since the objective function NS = 0.90 and the fit of goodness between simulation and observation R² is 0.82 (Figure 8c).

Table 7. Model performance During the Period 1990–2000.

Period	Average Monthly Flow (m ³ /s)		Standard Deviation (m ³ /s)		Model Performance			
	Measured	Simulated	Measured	Simulated	P-Factor	R-Factor	R ²	NS
Calibration (1990–1995)	172.28	161.79	234.95	212.24	0.97	0.83	0.82	0.9
Validation (1996–2000)	229.18	254.37	338.39	394.68	0.64	0.9	0.85	0.7

The average measured flow is 172.28 m³/s while the simulated was underestimated (161.79 m³/s). At the same time, simulated standard deviation (212.24 m³/s) was lower than the observed standard deviation (234.95 m³/s). For the validation performance of the model, the NS was 0.7 and the R² = 0.85 (Figure 7d) and can be classified as good. The mean monthly simulated flow was overestimated (254.37 m³/s) compared to the observed (229.18 m³/s). There is also difference in the standard deviation between simulated and observed flow. However, the difference is smaller compared to the first validation (Figure 7b). This can be a confirmation that the construction in the Bui dam impacts the dynamics of the river flow. The model was not able to capture the difference in flow regime. This may be explained by the fact that the reservoir was not included in the modeling process. In general, one can say that the Black Volta model has performed well despite uncertainties associated to the results.

3.4.3. Model Uncertainties

The SWAT model can be uncertain in its prediction of the hydrological processes. The lack of physical processes or parameters in the hydrological model seems to be responsible for the model errors. The degree to which all uncertainties are accounted for is quantified by a measure referred to as the P-factor, which is the percentage of measured data bracketed by the 95% prediction uncertainty (95PPU). In other words, the 95PPU is the degree to which all uncertainties are accounted for [46]. SUFI-2 accounts for all uncertainties including uncertainties in driving variable like rainfall, conceptual model, parameters and measured data (stream flow). P-factor is the percent of observations that are within the given uncertainty boundaries. The perfect situation would be 100% of the observed data bracketed in the 95PPU while at the same time the R-factor is close to zero for [46]. SUFI-2 accounts for all uncertainties including uncertainties in driving variable like rainfall, conceptual model, parameters and measured data. During the first calibration (2000–2005), 64% of the observed flow was bracketed in the 95PPU while the R-factor was 0.66 suggesting important uncertainties in the model. For the validation period (2006–2010), only 38% of the observed flow was barracked in the 95PPU and 0.33 as R-factor (see Table 6).

The uncertainties in the model during the second calibration and validation are reported in Table 7. During calibration (1990–1995) about 97% of the observed discharge were bracketed in the 95PPU suggesting a very good results or minimal uncertainties in the model. However, the R-factor was relatively high (0.83) meaning that the uncertainties cannot be neglected. The validation performance showed that uncertainties in the model are important (P-factor =64% and R-factor = 0.90). This may explain why the peak flows were not well captured during validation. Unfortunately, one cannot identify the source of uncertainties in the model.

3.4.4. Changes in Seasonal Stream Flow Due to LULC

The results of the intra-annual or seasonal variability analysis are shown in Table 8. The results are based on the long term simulation (1976–2011). The total flow of three months such as January, February and March were considered as dry period over the year for both LULC 2000 and 2013. The modeling of the dry period flow using the LULC of the year 2000 was 238.62 m³/s while the dry period flow using LULC of the year 2013 was 253.42 m³/s. The results showed that there is an increase of 6% in dry period flows due to LU practices in the Black Volta basin. Comparatively, wet period was defined considering the total flow of three months such as August, September and October. The stream

flow changes were also assessed due to land use changes in the catchments. The total flow for the wet period according to LULC 2000 was 2969.02 m³/s and 2995.35 m³/s for 2013 LULC. The results indicated that there was an increase by 1% in wet period stream flow. This stream flow assessment showed that it is important to monitor the land use practices in the basin since it has huge impact on river flow and by extension on the hydro-power generation at the Bui dam.

Table 8. Mean Monthly Flow.

LULC 2000		LULC 2013		Mean Monthly Flow Change	
Dry Months (Jan, Feb, Mar)	Wet Months (Aug, Sep, Oct)	Dry Months (Jan, Feb, Mar)	Wet Months (Aug, Sep, Oct)	Dry	Wet
238.62	2969.02	253.42	2995.35	+6%	+1%

3.4.5. Changes in Stream Flow Components Due to LULC

Primary investigation on the changes in the stream flow due to LULC showed strong impacts on stream flow. Further analysis focused on the stream flow components variability due to land use. The stream flow components including surface runoff (SURF_Q), lateral flow (LAT_Q), ground water contribution to stream flow (GW_Q) result in water yield. The effects of LULC on these elements are depicted in Table 9.

Table 9. Stream Flow Components Change Due to LULC.

Stream Flow Components (m ³ /s) and ET (mm)	LULC 2000	LULC 2013	Changes (%)
SURF_Q	376.7	477.3	27%
LAT_Q	5.7	6.8	19%
GW_Q	828	775.1	−6%
WATER_YIELD	1210.4	1259.2	4%
ET	521.6	546.7	4.59%

The results showed that with LULC 2000, the SURF Q, LAT Q and GW Q were respectively 376.7 m³/s, 5.7 m³/s and 828 m³/s while those with the LULC 2013 are respectively 477.3 m³/s, 6.8 m³/s and 775.1 m³/s. We have noticed that surface runoff and ground water are the big contributors to stream flow in the Black Volta catchment. We noticed that the components of stream flow are not affected in the same manner. For instance, between 2000 and 2013, the SURF_Q has increased by 27% while LAT_Q has increased by 19%. In contrast to the two other components, for the same period, GW_Q has decreased by −6%. The evapotranspiration (ET) has increased at the same time by 4.59%. These results can be explained by the fact that between the year 2000 and 2013, the urbanization rate and bare lands have increased respectively by 33.22% and 67.06%. At the same time, agricultural land has increased by 29.66% as an implication for the reduction in grass land by 44.54%. These results call for paying particular attention to ground water in the basin. The change in land use in terms of increasing urbanization and bare land have resulted in increasing surface runoff and reduced groundwater. The reduction in ground water contribution to stream flow may be due to the increase in ET when grass lands have been converted in crop lands. This may be due to difference in land use that controls ET.

4. Conclusions

In this paper, we discussed the spatio-temporal trend of rainfall and land use practices in their impacts on the Black Volta river discharge through the SWAT modeling. The statistics of the Mann-Kendall trend test showed that 61.4% of the rain gauges (8 stations over a total of 13) presented an increased precipitation trend whereas the rest of the stations showed a decreased trend. However, the test performed at the 95% confidence interval level showed that the detected trends in the rainfall

data were not statistically significant. The results showed that the rainfall variability is high across the basin. The standard precipitation index presents a succession of dry and wet years with a kind of recover from a rainfall deficit starting from the year 2000. Land use analysis showed significant deforestation mainly in the southern part of the Black Volta while the upper north is facing land degradation. The rate of urbanization ($2.37\% \text{ yr}^{-1}$ between 2000 and 2013) has direct impact on the hydrology of the basin. The SWAT modeling has shown good performance with relatively high Nash-Sutcliffe (NS) and coefficient of determination (R^2). The changes in seasonal stream flow due to land use have shown an increase by 6% and 1% respectively for wet and dry season between the year 2000 and 2013. Further analysis on the stream flow components revealed an increase in surface runoff by 27% but a decrease in groundwater contribution to stream flow by 6% between the year 2000 and 2013. On overall, there is an increase in water yield to stream flow by 4%. This could benefit the Bui hydropower plant. However, due to important land use change and high surface runoff, there is a need to properly monitor the water quality as well as sediment load in the river basin. Finally, for proper water management in the basin, an effort has to be made to increase the number of weather stations (only 13 stations in 130.000 km^2 were available).

Acknowledgments: We acknowledge with thanks the scholarship and financial support provided to me by BMBF, the Federal Ministry of Education and Research of Germany and the West African Science Service Center on Climate Change and Adapted Land Use (WASCAL). Special thanks to the Ghana Meteorological Agency (GMA) and la Direction General de la Meteorologie du Burkina Faso for providing us with the climate data. We are grateful to all other anonymous contributors and reviewers of this work.

Author Contributions: This paper is part of the correspondence author's master's thesis and the second and third authors were respectively first and second advisors. The first authors designed the research. The second author advised on the SWAT modeling and the third authors advised on the land use and land cover analysis.

Conflicts of Interest: The authors declare no conflict of interest. The founding sponsors had no role in the design of the study; in the collection, analyses, or interpretation of data; in the writing of the manuscript, and in the decision to publish the results.

Appendix A

Aridity Index

Global-Aridity is available as one grid layer representing the annual average over the 1950–2000 period. It is a high-resolution global raster climate data related to evapotranspiration processes and rainfall deficit for potential vegetative growth developed by (Zomer et al., 2008) [53]. Precipitation availability over atmospheric water demand can be quantified using an Aridity index. The data is a mean of AI from 1950–2000 period at 30 arc second ($\sim 1 \text{ km}$ at equator), spatial resolution. (Zomer et al., 2008) [53] expressed AI as:

$$(AI) = \frac{MAP}{MAE} \quad (A1)$$

where MAP is the Mean Annual Precipitation and MAE is the Mean Annual Potential Evapotranspiration (PET). The FAO defined PET as the evapotranspiration of a reference crop in optimal conditions having the following characteristics: well-watered grass with an assumed height of 12 cm, a fixed surface resistance of 70 s/m and an albedo of 0.23 [54]. The map is classified based on the generalized classification scheme of United Nations Environment Programme (UNEP), for Global Aridity values such as: <0.03 hyper arid zone, $0.03\text{--}0.2$ arid, $0.2\text{--}0.5$ semi-arid, $0.5\text{--}0.65$ dry sub humid and >0.65 humid.

Standardized Precipitation Index

The standardized precipitation index SPI_{sy} for each station was computed as:

$$SPI_{sy} = (P_{sy} - \bar{P}_s) / \sigma_s \quad (A2)$$

where P_{sy} is the annual rainfall of station s for year y , \bar{P}_s and σ_s are respectively the mean annual rainfall and the standard deviation of stations in the reference period 1976–2011. The annual index SP_y was then computed as an average of a certain number n of station that are in the same climatic zone that is defined from the aridity index profile as:

$$SPI_y = \frac{1}{n} \sum_{s=1}^n SPI_{sy} \quad (A3)$$

Mann-Kendall Trend Test

The theoretical calculation of the Mann-Kendall statistic S is given by:

$$S = \sum_{i=1}^{n-1} \sum_{j=i+1}^n \text{Sgn}(x_j - x_i) \quad (A4)$$

where n is the number of data points, X_i and X_j are the data values in time series i and j ($j > i$).

$\text{Sgn}(x_j - x_i)$ is the sign function defined as:

$$\text{Sgn}(x_j - x_i) = \begin{cases} +1, & \text{if } x_j - x_i > 0 \\ 0, & \text{if } x_j - x_i = 0 \\ -1, & \text{if } x_j - x_i < 0 \end{cases} \quad (A5)$$

The variance of the statistic S , $V(S)$ is defined as:

$$V(S) = \frac{n(n-1)(2n+5) - \sum_{i=1}^q t_i(t_i-1)(2t_i+5)}{18} \quad (A6)$$

Again n is the number of data points, q is the number of the tied groups and t_i is the number of data values in the i th group. Tied group can be defined as group of sample data which have the same value. When $n > 10$, a standardized statistic Z_S is calculated as bellow:

$$Z_S = \begin{cases} \frac{S-1}{\sqrt{V(S)}}, & \text{if } S > 0 \\ 0, & \text{if } S = 0 \\ \frac{S+1}{\sqrt{V(S)}}, & \text{if } S < 0 \end{cases} \quad (A7)$$

Positive value of Z_S indicates upward trend and negative value of Z_S indicates downward trend. The testing trend is done at a specific α level. The alpha level considered in this study $\alpha = 0.05$ is which correspond to confidence level of 95%. The null hypothesis H_0 is rejected when $|Z_S| > Z_{1-\alpha/2}$ implying significant trend in the time series data (Either increase when $Z_S > Z_{1-\alpha/2}$ or decrease when $Z_S < -Z_{1-\alpha/2}$); H_0 is accepted which implies there is no trend in the rainfall time series data [30]. $Z_{1-\alpha/2}$ is given by the standard normal distribution table. For this study $\alpha = 0.05$ with $Z_{1-\alpha/2} = 1.96$ is considered. Another parameter considered in the Mann-Kendall test is Kendall's tau [55]. The tau value is considered as the slope and varies between -1 and $+1$. A negative value of tau indicates decreasing trend and positive value indicates increasing trend. Before the application of Mann-Kendall test for trend detection in the rainfall time series data at annual level, it is important to investigate if the data is serial correlated. For this study, the serial correlation of the data was investigated using the acf (autocorrelation) and pacf (partial autocorrelation) function in R package by [35] showed no serial correlation in the dataset.

Sen's Slope Estimator

The linear model $f(t)$ can be described as:

$$f(t) = Qt + B \quad (\text{A8})$$

where Q is the slope B is a constant. To derive an estimate of the slope Q , the slopes of all data pairs are calculated as:

For N pair of data in the sample, the slope is:

$$Q_i = \frac{x_j - x_k}{j - k} \text{ for } i = 1, \dots, N \quad (\text{A9})$$

where x_j and x_k are data values at time j and k ($j > k$) respectively. The median Q_{med} of N values of Q_i is the Sen's slope estimator. The median is calculated as the Equation (A10):

$$Q_{\text{med}} = \begin{cases} Q_{[(n+1)/2]} & \text{if } N \text{ is odd} \\ \frac{1}{2}(Q_{[N/2]} + Q_{[(N+2)/2]}) & \text{if } N \text{ is even} \end{cases} \quad (\text{A10})$$

The two tailed test is used to test the significance of the median Q_{med} at a specific alpha level. In this study, $\alpha = 0.05$ is used. The Q_{med} value and sign represent the steepness and the trend of the data. The confidence interval for this value is computed as:

$$C_\alpha = Z_{1-\alpha/2} \sqrt{V(S)} \quad (\text{A11})$$

With $V(S)$ the variance of the Mann-Kendall statistic S defined in the Equation (A8) while $Z_{1-\alpha/2}$ is obtained from the standard normal distribution table. Furthermore, $M_1 = (N - \alpha) / 2$ and $M_2 = (N + \alpha) / 2$ are computed. The lower and upper limits of the confidence interval, Q_{min} and Q_{max} , are the M_1 th largest and $(M_2 + 1)$ th largest of the N ordered slope estimates [56]. For this work, the Sen's slope estimator was computed in R software using the Package 'wq' [57].

References

- Oguntunde, P.G.; Friesen, J.; van de Giesen, N.; Savenije, H.H.G. Hydroclimatology of the Volta River Basin in West Africa: Trends and variability from 1901 to 2002. *Phys. Chem. Earth* **2006**, *31*, 1180–1188. [CrossRef]
- Conway, D.; Persechino, A.; Ardoin-Bardin, S.; Hamandawana, H.; Dieulin, C.; Mahé, G. Rainfall and Water Resources Variability in Sub-Saharan Africa during the Twentieth Century. *J. Hydrometeorol.* **2009**, *10*, 41–59. [CrossRef]
- Mahe, G.; L'Hote, Y.; Olivry, J.C.; Wotling, G. Trends and discontinuities in regional rainfall of West and Central Africa: 1951–1989. *Hydrol. Sci. J.* **2001**, *46*, 211–226. [CrossRef]
- Owusu, K.; Waylen, P. Trends in spatio-temporal variability in annual rainfall in Ghana (1951–2000). *Weather* **2009**, *64*, 115–120. [CrossRef]
- Logah, F.Y.; Obuobie, E.; Ofori, D.; Kankam-Yeboah, K. Analysis of Rainfall Variability in Ghana. *Int. J. Latest Res. Engineer. Comput.* **2013**, *1*, 1–8.
- Lacombe, G.; McCartney, M.; Forkuor, G. Drying climate in Ghana over the period 1960–2005: Evidence from the resampling-based Mann-Kendall test at local and regional levels. *Hydrol. Sci. J.* **2012**, *57*, 1594–1609. [CrossRef]
- Andreini, M.; van de Giesen, N.; van Edig, A.; Fosu, M.; Andah, W. *Volta Basin Water Balance*; ZEF: Bonn, Germany, 2000.
- Arnold, J.G.; Kiniry, J.R.; Srinivasan, R.; Williams, J.R.; Haney, E.B.; Neitsch, S.L. *Soil and Water Assessment Tool, Input/output File Documentation*; Technical Report 439; Texas Water Research Institute: College Station, TX, USA, 2012.
- Neitsch, S.L.; Arnold, J.G.; Kiniry, J.R.; Srinivasan, R.; Williams, J.R. *Soil and Water Assessment Tool Input/Output File Documentation*; Blackland Research Center: Temple, TX, USA, 2005.

10. Setegn, S.G.; Srinivasan, R.; Dargahi, B. Hydrological modelling in the Lake Tana Basin, Ethiopia using SWAT model. *Open Hydrol. J.* **2008**, *2*, 49–62. [[CrossRef](#)]
11. Malunjar, V.S.; Shinde, M.G.; Ghotekar, S.S.; Atre, A.A. Estimation of Surface Runoff using SWAT Model. *Int. J. Latest Res. Engineer. Comput.* **2015**, *3*, 12–15.
12. Easton, Z.M.; Fuka, D.R.; White, E.D.; Collick, A.S.; Ashagre, A.B.; McCartney, M.; Awulachew, S.B.; Ahmed, A.A.; Teenhuis, T.S. A multi basin SWAT model analysis of runoff and sedimentation in the Blue Nile, Ethiopia. *Hydrol. Earth System Sci.* **2010**, *14*, 1827–1841. [[CrossRef](#)]
13. Spruill, C.A.; Workman, S.R.; Taraba, J.L. Simulation of Daily and Monthly Stream Discharge from Small Watershed Using the SWAT Model. *Am. Soc. Agric. Eng.* **2000**, *1*, 1431–1439. [[CrossRef](#)]
14. Awotwi, A.; Kumi, M.; Pe, J.; Yeboah, F.; Nti, I.K. Predicting Hydrological Response to Climate Change in the White Volta. *J. Earth Sci. Clim. Chang.* **2015**, *6*, 1–7. [[CrossRef](#)]
15. Obuobie, E. *Estimation of Groundwater Recharge in the Context of Future Climate Change in the White Volta River Basin, West Africa*; ZEF: Bonn, Germany, 2008.
16. Schuol, J.; Abbaspour, K.C. Calibration and uncertainty issues of a hydrological model (SWAT) applied to West Africa. *Adv Geosci.* **2006**, *2*, 137–143. [[CrossRef](#)]
17. Allwaters Consult. *Diagnostic Study of The Black Volta Basin in Ghana*; Final Report; ALLWATERS Consult Limited: Kumasi, Ghana; June; 2012.
18. Green Cross International, Burkina Faso, 2001. Trans-boundary Basin Sub-Projects: The Volta River Basin. Available online: www.greencrossitalia.it/ita/acqua/wfp/pdf/greencrosswfp_volta.pdf (accessed on 15 January 2016).
19. Barry, B.; Obuobie, E.; Andreini, M.; Andah, W.; Pluquet, M. *The Volta River Basin: Comparative Study of River Basin Development and Management. Comprehensive Assessment of Water Management in Agriculture*; IWMI: Colombo, Sri Lanka, 2005.
20. Shaibu, S.; Odai, S.N.; Adjei, K.A.; Osei, E.M.; Annor, F.O. Simulation of runoff for the Black Volta Basin using satellite observation data. *Int. J. River Basin Manag.* **2012**, *10*, 245–254. [[CrossRef](#)]
21. Peterson, T.C.; Easterling, D.R.; Karl, T.R.; Groisman, P.; Nicholls, N.; Plummer, N.; Vincent, L. Homogeneity adjustments of *in situ* atmospheric climate data: A review. *Int. J. Climatol.* **1998**, *18*, 1493–1517. [[CrossRef](#)]
22. Reeves, J.; Chen, J.; Wang, X.L.; Lund, R.; Lu, Q.Q. A review and comparison of changepoint detection techniques for climate data. *J. Appl. Meteorol. Climatol.* **2007**, *46*, 900–915. [[CrossRef](#)]
23. Searcy, J.K.; Hardison, C.H. *Double-Mass Curves*; US Government Printing Office: Washington, WA, USA, 1960.
24. Westmacott, J.R.; Burn, D.H. Climate change effects on the hydrologic regime within the Churchill-Nelson River Basin. *J. Hydrol.* **1997**, *202*, 263–279. [[CrossRef](#)]
25. Cannarozzo, M.; Noto, L.V.; Viola, F. Spatial distribution of rainfall trends in Sicily (1921–2000). *Phys. Chem. Earth* **2006**, *31*, 1201–1211. [[CrossRef](#)]
26. Liu, Q.; Yang, Z.; Cui, B. Spatial and temporal variability of annual precipitation during 1961–2006 in Yellow River Basin, China. *J. Hydrol.* **2008**, *361*, 330–338. [[CrossRef](#)]
27. Zhang, Y.; Guan, D.; Jin, C.; Wang, A.; Wu, J.; Yuan, F. Analysis of impacts of climate variability and human activity on streamflow for a river basin in northeast China. *J. Hydrol.* **2011**, *410*, 239–247. [[CrossRef](#)]
28. Gocic, M.; Trajkovic, S. Analysis of changes in meteorological variables using Mann-Kendall and Sens slope estimator statistical tests in Serbia. *Glob. Planet. Chang.* **2013**, *100*, 172–182. [[CrossRef](#)]
29. Lanzante, J.R. Resistant, Robust and Non-Parametric Techniques for the Analysis of Climate Data: Theory and Examples, Including Applications to Historical Radiosonde Station Data. *Int. J. Climatol.* **1996**, *16*, 1197–1226. [[CrossRef](#)]
30. Kendall, M.G. *Rank Correlation Methods*; Hafner Press: New York, NY, USA, 1962.
31. Ahmad, I.; Tang, D.; Wang, T.; Wang, M.; Wagan, B. Precipitation Trends over Time Using Mann-Kendall and Spearman’s Rho Tests in Swat River Basin, Pakistan. *Adv. Meteorol.* **2015**, Article ID 431860. [[CrossRef](#)]
32. Hirsch, R.M.; Alexander, R.B.; Smith, R.A. Selection of methods for the detection and estimation of trends in water quality. *Water Resour. Res.* **1991**, *27*, 803–813. [[CrossRef](#)]
33. Tabari, H.; Marofi, S.; Aeini, A.; Talaei, P.H.; Mohammadi, K. Trend analysis of reference evapotranspiration in the western half of Iran. *Agric. For. Meteorol.* **2011**, *151*, 128–136. [[CrossRef](#)]
34. Bayazit, M.; Önöz, B.; Yue, S.; Wang, C. Comment on “Applicability of prewhitening to eliminate the influence of serial correlation on the Mann-Kendall test” by Sheng Yue and Chun Yuan Wang. *Water Resour. Res.* **2004**, *40*, 1–5. [[CrossRef](#)]

35. Sen, P.K. Estimates of the Regression Coefficient Based on Kendall's Tau. *J. Am. Stat. Assoc.* **1968**, *63*, 1379–1389. [[CrossRef](#)]
36. Van Vliet, J.; Bregt, A.K.; Hagen-Zanker, A. Revisiting Kappa to account for change in the accuracy assessment of land-use change models. *Ecol Modell.* **2011**, *222*, 1367–1375. [[CrossRef](#)]
37. Stehman, S.V.; Czaplewski, R.L. Design and Analysis for Thematic Map Accuracy Assessment—An application of satellite imagery. *Remote Sens. Environ.* **1998**, *64*, 331–344. [[CrossRef](#)]
38. Foody, G.M. Status of land cover classification accuracy assessment. *Remote Sens. Environ.* **2002**, *80*, 185–201. [[CrossRef](#)]
39. Zăvoianu, F.; Caramizoiub, A.; Badeaa, D. Study and Accuracy Assessment of Remote Sensing Data for Environmental Change Detection in Romanian Coastal Zone of the Black Sea. In Proceedings International Society for Photogrammetry and Remote Sensing, Istanbul, Turkey, 12–23 July 2004.
40. Carletta, J. Assessing agreement on classification tasks: The kappa statistic. *Comput. Linguist.* **1996**, *22*, 249–254.
41. Neitsch, S.L.; Williams, J.R.; Arnold, J.G.; Kiniry, J.R. *Soil and Water Assessment Tool Theoretical Documentation*; Version 2009; Texas Water Resources Institute: College Station, TX, USA, 2011.
42. United States. Soil Conservation Service. *Hydrology. SCS National Engineering Handbook*; U.S Department of Agriculture: Washington, WA, USA, 1972. Section 4.
43. Green, W.H.; Ampt, G.A. Studies on Soil Physics. *J. Agric. Sci.* **1911**, *4*, 1. [[CrossRef](#)]
44. NRCS. *Urban Hydrology for Small Watersheds TR-55*; U.S Department of Agriculture: Washington, WA, USA, 1986.
45. Abbaspour, K.C.; Vejdani, M.; Haghighat, S.; Yang, J. SWAT-CUP Calibration and Uncertainty Programs for SWAT. *Fourth Int. SWAT Conf.* **2007**, 1596–1602.
46. Abbaspour, K.C.; Johnson, C.A.; van Genuchten, M.T. Estimating Uncertain Flow and Transport Parameters Using a Sequential Uncertainty Fitting Procedure. *Vadose Zone J.* **2004**, *3*, 1340–1352. [[CrossRef](#)]
47. Nash, J.E.; Sutcliffe, J.V. River flow forecasting through conceptual models part I—A discussion of principles. *J. Hydrol.* **1970**, *10*, 282–290. [[CrossRef](#)]
48. Abbaspour, K.C. *SWAT-CUP 2012: SWAT calibration and uncertainty Programs-A user manual*; Eawag (Swiss Federal Institute of Aquatic Science and Technology): Zurich, Switzerland, 2013. Available online: swat.tamu.edu/media/114860/usermanual_swatcup.pdf (accessed on 29 June 2016).
49. Moriasi, D.; Arnold, J. Model evaluation guidelines for systematic quantification of accuracy in watershed simulations. *Trans. ASABE* **2007**, *50*, 885–900. [[CrossRef](#)]
50. L'Hôte, Y.; Mahé, G.; Somé, B.; Triboulet, J.P. Analysis of a Sahelian annual rainfall index from 1896 to 2000; the drought continues. *Hydrol. Sci. J.* **2002**, *47*, 563–572. [[CrossRef](#)]
51. Anderson, J.R. *A land use and land cover classification system for use with remote sensor data*. US Government Printing Office: Washington, WA, USA, 1976.
52. Adjei, K.A.; Ren, L.; Appiah-adjei, E.K.; Odai, S.N. Application of satellite-derived rainfall for hydrological modelling in the data-scarce Black Volta trans-boundary basin. *Hydrol. Res.* **2015**, *46*, 777–791. [[CrossRef](#)]
53. Zomer, R.J.; Trabucco, A.; Bossio, D.A.; Verchot, L.V. Climate change mitigation: A spatial analysis of global land suitability for clean development mechanism afforestation and reforestation. *Agric. Ecosyst. Environ.* **2008**, *126*, 67–80. [[CrossRef](#)]
54. Allen, R.G.; Pereira, L.S.; Raes, D.; Smith, M. *Crop Evapotranspiration-Guidelines for Computing Crop Water Requirements-FAO Irrigation and Drainage Paper 56*; FAO: Rome, Italy, 1998.
55. Mcleod, A.A.I. Kendall rank correlation and Mann-Kendall trend test. Available online: <https://cran.r-project.org/web/packages/Kendall/> (accessed on 25 June 2016).
56. Hollander, M.; Wolfe, D.A.; Chicken, E. *Nonparametric Statistical Methods*; John Wiley & Sons: Hoboken, NJ, USA, 2013.
57. Jassby, A.D.; Cloern, J.E. wq: Exploring water quality monitoring data. Available online: <https://www.icesi.edu.co/CRAN/web/packages/wq/> (accessed on 25 June 2016).

